Annals of Nuclear Medicine
https://doi.org/10.1007/s12149-019-01341-0

ORIGINAL ARTICLE

Development of a p38α-selective radioactive probe for qualitative diagnosis of cancer using SPECT

Masahiko Hirata[1] · Tatsuma Yao[1] · Shigeaki Fujimura[1] · Yasukazu Kanai[1] · Mitsuyoshi Yoshimoto[1,2] · Takaji Sato[1] · Yoshiro Ohmomo[1] · Takashi Temma[1]

Received: 7 December 2018 / Accepted: 23 January 2019

Abstract

Objective p38 mitogen-activated protein (MAP) kinase (p38α) has drawn attention as a new target molecule for the treatment and diagnosis of cancer, and its overexpression and activation have been reported in various types of cancer. In this study, a single photon emission computed tomography (SPECT) imaging probe of p38α was developed to noninvasively image p38α activity for effective qualitative diagnosis of cancer.

Methods Pyrrolepyridine derivatives, *m*-YTM and *p*-YTM, were designed and synthesized based on the structure of the p38α-selective inhibitor. Radioactive iodine-labeled *m*-YTM, [^{125}I]*m*-YTM, was synthesized because *m*-YTM greatly inhibited the phosphorylation of p38α upon examining the inhibitory effects of the compounds. After investigating the binding affinity of [^{125}I]*m*-YTM to the recombinant p38α, a saturation binding experiment using activated p38α and inactive p38α was performed to determine the binding site. Uptake of [^{125}I]*m*-YTM into various cancer cell lines was investigated, and the pharmacokinetics was evaluated using tumor-bearing mice.

Results The inhibitory activity of *m*-YTM was approximately 13 times higher than that of SB203580, a p38α-selective inhibitor. The binding site of [^{125}I]*m*-YTM was estimated to be the p38α activating site, similar to that of SB203580, because the [^{125}I]*m*-YTM bound strongly to both activated p38α and inactive p38α. Various different cancer cells incorporated [^{125}I]*m*-YTM; however, its accumulation was significantly reduced by treatment with SB203580. Pharmacokinetics study of [^{125}I]*m*-YTM in B-16 tumor-bearing mice was examined which revealed high accumulation of radioactivity in tumor tissues. The ratios of radioactivity in the B-16 tumor to that in blood were 3.1 and 50 after 1 and 24 h, respectively. The ratio of radioactivity in the tumor to that in blood in the tumor-bearing mice generated using other cancer cell lines was also ≥ 1 at 1 h after the administration of the probe.

Conclusions This study suggests that [^{123}I]*m*-YTM has potential as a p38α imaging probe effective for various cancer types.

Keywords P38α · Tumor imaging · SPECT

Introduction

Mitogen-activated protein (MAP) kinase is an intracellular signaling kinase found in mammalian culture cells; it is a serine/threonine kinase commonly activated by various growth factors, which was discovered in the late 1980s. It is functionally involved in various biological activities, such as cellular growth and differentiation, cell death, cell cycle suppression, early development, and brain diseases [1, 2]. MAP kinase is considered to be activated in response to external stimuli, after which it moves to the nucleus to regulate gene expression through the phosphorylation of transcription factors, among others.

The activation of MAP kinase requires the phosphorylation of threonine/tyrosine residues in the TEY (Thr–Glu–Tyr) sequence between subdomains VII and VIII of the kinase. Enzymes that phosphorylate both amino acid residues and activate MAP kinase are serine/threonine/tyrosine kinases, MAP kinase kinases (MAPKK,

✉ Takashi Temma
ttemma@gly.oups.ac.jp

[1] Department of Biofunctional Analysis, Osaka University of Pharmaceutical Sciences, 4-20-1 Nasahara, Takatsuki, Osaka 569-1094, Japan

[2] Division of Functional Imaging, Exploratory Oncology Research & Clinical Trial Center, National Cancer Center, Kashiwa, Chiba, Japan

Published online: 05 April 2019

MEK). The activation of MAPKK itself also requires the phosphorylation of serine/threonine residues, and enzymes that phosphorylate MAPKK are called MAPKK kinases (MAPKKK). This cascade composed of three different kinases, namely, MAP kinase, MAPKK, and MAPKKK, is called an MAP kinase cascade. In addition, a group of MAP kinases carrying a TPY (Thr-Pro-Tyr) sequence or a TGY (Thr-Gly-Tyr) sequence instead of the TEY sequence and requiring the phosphorylation of threonine and tyrosine residues for their activation has been discovered; these are collectively referred to as MAP kinase superfamily molecules [3].

p38 is a MAP kinase family molecule requiring the phosphorylation of threonine and tyrosine residues in the TGY sequence for its activation; currently, four genes encoding having this sequence have been identified: p38α, p38β, p38γ, and p38δ [4]. p38α is known to be activated in response to stimuli such as inflammatory cytokines and is involved in processes such as apoptosis [5, 6]. Aberrant activation of p38α is observed in the early stages of ischemic diseases, such as myocardial infarction [7–9] and cerebral infarction [10, 11], and it has been reported that cell death due to ischemia can be prevented by inhibiting this abnormal activity of p38α using the p38-selective inhibitor SB203580 [8, 12, 13]. Urokinase plasminogen activator (uPA) and its receptor uPA receptor, which are involved in the infiltration and metastasis of tumor cells, are known to show increased levels in many cancers [14], and continuous activation of p38α has been found to be necessary for this expression [15, 16]. Recently, p38α is recognized as a potential therapeutic target in tumors [17, 18].

Based on the evidence described above, we decided to develop a novel radiopharmaceutical for p38α activity diagnosis because, if aberrant activity of p38α could be revealed from outside the body, it would enable early detection of the aforementioned diseases, which would be very useful for their diagnosis and treatment. *m*-YTM and *p*-YTM (Fig. 1) were designed based on the structure–activity relationship of 6-amino-2-(4-fluorophenyl)-4-benzyloxy-3-(4-pyridyl)-1H-pyrrolo[2,3-b]pyridine (RWJ-15) [19] with p38α, and synthesized. Subsequently, because *m*-YTM exhibited high inhibitory activity, its radioactive iodine-labeled form was synthesized. The compound obtained was examined in vitro and in vivo to evaluate its effectiveness as a novel SPECT imaging probe for detecting p38α activity.

Fig. 1 Drug design of *m*-YTM and *p*-YTM as a novel p38α imaging probe

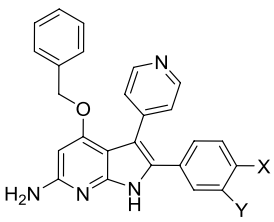

X=H, Y=I: *m*-YTM
X=I, Y=H: *p*-YTM
X=F, Y=H: RWJ-15

Methods

Reagents and instruments

The radioactive compounds [^{125}I]sodium iodide and [γ-^{32}P]ATP were purchased from Amersham Pharmacia Biotech Inc. Fetal calf serum (FCS), penicillin–streptomycin solution, and MEMα were purchased from Trace Biosciences Pty. Ltd., Wako Chemicals, and Nacalai Tesque, respectively. p38α (active, inactive) was obtained from Upstate Biotechnology; SB203580, SB202190, SB202474, PD98059, U0126, Go6983, and bisindolylmaleimide I were from Calbiochem; and SP600125 was from Tocris. All other reagents obtained were of special grade and used without purification.

Melting point was measured with a Yanagimoto micro-melting point apparatus. IR spectra were measured with the IR-700 (JASCO Corporation). ^{1}H-NMR spectra were measured with the Mercury-300 (Varian) and chemical shifts were reported in δ (ppm) values using tetramethylsilane as an internal standard. High-resolution mass spectra (HRMS) were measured with M-80 or DIP-181 (JASCO Corporation). A CK-40 microscope (Olympus) was employed. Absorbance was measured using Model 550 Microplate Reader (Bio-Rad). HPLC was performed using a device composed of a 600C type pump, 600F type universal injector, 2487 type detector (Waters), 170 type I detector (Beckman), C-18 reverse-phase column (10 × 25 mm; Nacalai Tesque), and a mobile phase of methanol/water (80:20, v/v) at a flow rate of 3 ml/min to measure absorbance (254 nm) and ^{125}I radioactivities. Radioactivities of ^{125}I were measured using an ARC-300 or ARC-380 auto-well gamma counter (Aloka). Radioactivities of ^{32}P were measured with a TRI-CARB1600CA type liquid scintillation analyzer (Packard).

A-375 cells were obtained from the University of Fukui Biomedical Imaging Research Center. B-16, C-6, SLC, ME-180, PC-3, and A-431 cell lines were provided by the Cell Resource Center for Biomedical Research, Institute of Development, Aging and Cancer, Tohoku University. Mice were purchased from Japan SLC and raised in accordance with Osaka University of Pharmaceutical Sciences animal experiment guidelines.

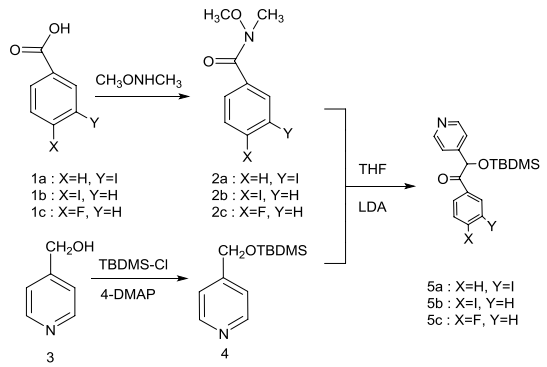

Scheme 1 Synthesis of compounds 1–5

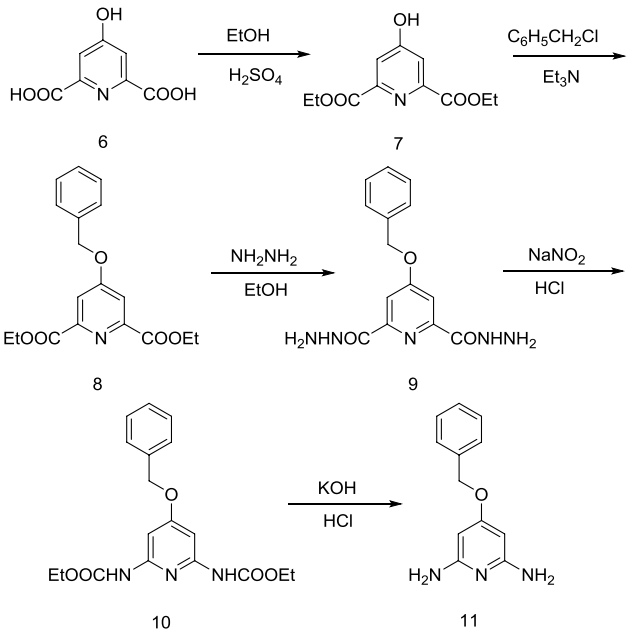

Scheme 2 Synthesis of compounds 6–11

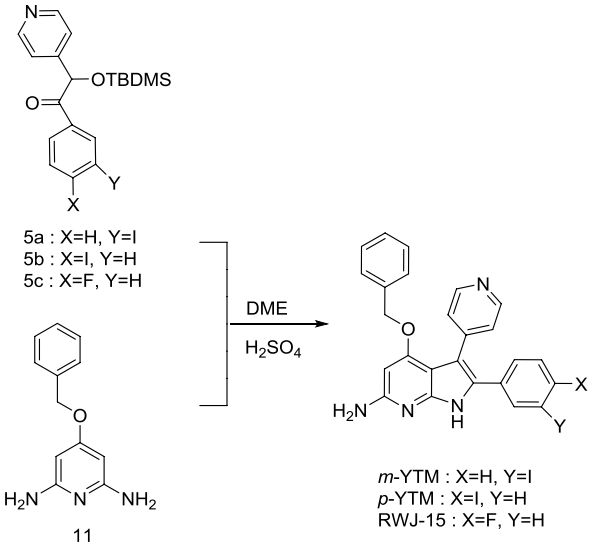

Scheme 3 Synthesis of *m*-YTM, *p*-YTM, and RWJ-15

Synthesis (Schemes 1, 2, 3)

m-Iodo-*N*-methoxy-*N*-methyl-benzamide (2a)

m-Iodo benzoic acid (**1a**) (4.0 g, 0.0162 mol) was dissolved in thionyl chloride (6.8 mL) and then refluxed for 2 h. After evaporating the reaction mixture under reduced pressure, the mixture was added dropwise to a mixed solution of anhydrous DMF (100 mL) and *N,O*-dimethylhydroxylamine hydrochloride (16.0 g, 0.1640 mol) and refluxed for 12 h. Next, after evaporating the solvent under reduced pressure, water (100 mL) was added to the residue and the pH of the mixture was adjusted to 11 with 2 M NaOH. Subsequently, after extracting with chloroform (100 mL × 2), the extract was washed with water (100 mL × 2). The organic layer was dried over sodium sulfate, and then the solvent was distilled off under reduced pressure. The residue was separated and purified by silica gel column chromatography using chloroform as an eluate to obtain **2a** as an oily matter.

Yield 57.5%. ^{1}H–NMR ($CDCl_3$): 3.35 (s, 3H, C$\underline{H}_3$), 3.55 (s, 3H, OC$\underline{H}_3$), 7.14 (t, J = 8.1 Hz, 1H, aromatics), 7.64 (d, J = 8.1 Hz, 1H, aromatics), 7.78 (d, J = 8.1 Hz, 1H, aromatics), 8.01 (s, 1H, aromatics). HRMS: m/z 290.9756. Found: 290.9756. Anal. calcd. for $C_9H_{10}INO_2$: C, 37.14; H, 3.46; N, 4.81. Found: C, 36.94; H, 3.47; N, 4.89.

p-Iodo-*N*-methoxy-*N*-methyl-benzamide (2b)

Using *p*-iodo benzoic acid (**1b**), it was synthesized in a manner similar to that used for synthesizing **2a**.

Yield 45.7%. ^{1}H–NMR ($CDCl_3$): 3.34 (s, 3H, C$\underline{H}_3$), 3.53 (s, 3H, OC$\underline{H}_3$), 7.43 (d, J = 8.4 Hz, 2H, aromatics), 7.75 (d, J = 8.4 Hz, 2H, aromatics). HRMS: m/z 290.9756. Found: 290.9756. Anal. calcd. for $C_9H_{10}INO_2$: C, 37.14; H, 3.46; N, 4.81. Found: C, 36.93; H, 3.38; N, 4.92.

p-Fluoro-*N*-methoxy-*N*-methyl-benzamide (2c)

Using *p*-fluoro benzoic acid (**1c**), it was synthesized in a manner similar to that used for synthesizing **2a**.

Yield 43.2%. ^{1}H–NMR ($CDCl_3$): 3.36 (s, 3H, C$\underline{H}_3$), 3.54 (s, 3H, OC$\underline{H}_3$), 7.08 (d, J = 8.4 Hz, 2H, aromatics), 7.74 (d, J = 8.4 Hz, 2H, aromatics).

4-(*tert*-Butyl-dimethyl-silanyloxymethyl)-pyridine [4]

4-Pyridinemethanol [3] (10 g, 0.0916 mol), 4-dimethylaminopyridine (5.8 g, 0.0474 mol), and *tert*-butyldimethylchlorosilane (15.2 g, 0.1008 mol) were dissolved in

chloroform (190 mL). After triethylamine was added dropwise (15.2 mL, 0.1096 mol) into the solution, it was stirred at room temperature for 3 h.

After washing with water (100 mL × 3) and drying the organic layer over sodium sulfate, the solvent was evaporated under reduced pressure. The residue was separated and purified by silica gel column chromatography using chloroform/methanol (100/1, v/v) as an eluate to obtain **4** as an oily matter.

Yield 82.5% ^{1}H–NMR ($CDCl_3$): 0.20 (s, 6H, C$\underline{H}_3$), 1.05 (s, 9H, C$\underline{H}_3$), 4.82 (s, 2H, OC$\underline{H}_2$), 7.33 (d, J = 6.0 Hz, 2H, aromatics), 8.62 (d, J = 6.0 Hz, 2H, aromatics). MS: m/z 223. Found: 223.

2-(*tert*-Butyl-dimethyl-silanyloxy)-1-(3,4-iodo,4-fluorophenyl)-2-pyridin-4-yl-ethanone (5a–c) Under conditions with an argon stream and a temperature of − 78 °C, **4** (2.1 g, 0.0094 mol) was dissolved in THF (40 mL) to which LDA (7.9 mL, 0.0158 mol) was slowly added dropwise over 1 h. Following stirring for 1 h, a solution in which **2a–c** (2.3 g, 0.0079 mol) was dissolved in THF (10 mL) was added dropwise over 1 h and stirred for 15 min. After evaporation under reduced pressure, a small amount of chloroform and water was added, and the precipitated impurities were filtered. After extracting with chloroform (100 mL × 3), the product was washed with brine (100 mL × 3), dried over sodium sulfate, and evaporated under reduced pressure. The fraction of **5a–c** was separated by silica gel column chromatography using chloroform as an eluate and was used without purification.

4-Hydroxy-pyridine-2,6-dicarboxylic acid diethyl ester [7]

Chelidamic acid [6] (10.0 g, 0.0546 mol) was added to ethanol (150 mL), after which sulfuric acid (1.0 mL) was added dropwise; the solution was then refluxed overnight. After evaporating under reduced pressure, the reaction was extracted with chloroform (100 mL × 3), washed with water (50 mL × 2), dried over sodium sulfate, and evaporated under reduced pressure. The residue was recrystallized with ethanol to obtain **7** in the form of white crystals.

Yield 46.2%. mp 120–121 °C. ^{1}H–NMR ($CDCl_3$): 1.33 (t, J = 7.2 Hz, 6H, C$\underline{H}_3$), 4.35 (q, J = 7.2 Hz, 4H, C$\underline{H}_2$), 7.57 (s, 2H, aromatics), 11.57 (broad s, 1H, OH). MS: m/z 239. Found: 239.

4-Benzyloxy-pyridine-2,6-dicarboxylic acid diethyl ester [8]

In THF (30 mL), **7** (1.5 g, 0.00627 mol) was dissolved, then triethylamine (8.25 mL, 0.006 mol) was added, and the mixture was stirred at room temperature for 30 min. Subsequently, benzylchloride (5.5 mL) was added dropwise and the mixture was refluxed overnight. The resulting precipitate was removed by suction filtration, and the reaction solution was evaporated under reduced pressure. After extracting with chloroform (30 mL × 2) and washing with water (30 mL × 2), the organic layer was dried over sodium sulfate and evaporated under reduced pressure. The residue was separated and purified by silica gel column chromatography using ether/hexane (1/1, v/v) as an eluate to obtain **8** as white crystals.

Yield 54.2%. mp 79–81 °C, lit [20], mp 79–81 °C. ^{1}H–NMR ($CDCl_3$): 1.45 (t, J = 7.2 Hz, 6H, C$\underline{H}_3$), 4.47 (q, J = 7.2 Hz, 4H, C$\underline{H}_2$), 5.22 (s, 2H, OC$\underline{H}_2$), 7.43 (m, 5H, aromatics), 7.86 (s, 2H, aromatics). MS: m/z 329. Found: 329.

4-Benzyloxy-pyridine-2,6-dicarboxylic acid dihydrazide [9]

In ethanol (260 mL), **8** (18.3 g, 0.0555 mol) was dissolved, and after adding hydrazine monohydrate (23 mL, 0.474 mol) dropwise, the solution was refluxed for 2 h. The reaction solution was cooled and the precipitate was suction filtered to obtain **9** as white crystals.

Yield 95.6%. mp 206–208 °C, lit [20], mp 206–208.5 °C. ^{1}H–NMR (DMSO): 4.62 (d, J = 4.2 Hz, 4H, N$\underline{H}_2$), 5.35 (s, 2H, OC$\underline{H}_2$), 7.40 (m, 5H, aromatics), 7.67 (s, 2H, aromatics), 10.59 (t, J = 4.2 Hz, 2H, N$\underline{H}$). MS: m/z 301. Found: 301.

4-Benzyloxy-2,6-dicarboethoxyamino pyridine [10]

In 1 M HCl solution (60 mL), **9** (3 g, 0.01 mol) was added, and a solution in which $NaNO_2$ (2.8 g, 0.04 mol) was dissolved in a mixture of DMF/water (2/1, v/v) (21 mL) was slowly added dropwise and kept at 10–15 °C. The resulting gummy product was removed, and benzene and brine were added. After extraction and washing with water, the organic layer was dried over sodium sulfate and evaporated under reduced pressure. The residue was thoroughly dried, then added to ethanol (110 mL), refluxed for 1 h, and then evaporated under reduced pressure. The product was extracted with chloroform, washed with water, and the organic layer was dried over sodium sulfate and evaporated under reduced pressure. The residue was separated and purified by silica gel column chromatography using chloroform as an eluate to obtain **10** as a gummy matter.

Yield 44.01%. mp 118–120 °C, lit [20], mp 118–120 °C. ^{1}H–NMR ($CDCl_3$): 1.31 (t, J = 7.2 Hz, C$\underline{H}_3$), 4.24 (q, J = 7.2 Hz, 4H, C$\underline{H}_2$), 5.14 (s, 2H, OC$\underline{H}_2$), 7.40 (m, 7H, aromatics), 8.33 (s, 2H, N$\underline{H}$). MS: m/z 359. Found: 359.

4-Benzyloxy-2,6-diaminopyridine [11]

After dissolving **10** (2.53 g, 0.007 mol) in ethanol (100 mL), an ethanol solution of KOH (2.53 g, 0.045 mol) (40 mL) was

added dropwise, and then the solution was refluxed for 12 h. After completion of the reaction, the precipitate formed by cooling was removed by filtration. The filtrate was adjusted to an acidic state (pH 3) by adding 1 M HCl aqueous solution, followed by refluxing for 30 min. The solution was then adjusted to a basic state (pH 11) by slowly adding 1 M NaOH aqueous solution, followed by evaporation under reduced pressure. Water (30 mL) was added to the residue, after which the solution was extracted with ethyl acetate (100 mL × 3), dried over sodium sulfate, evaporated under reduced pressure, and separated and purified by silica gel column chromatography using chloroform/methanol (10/1, v/v) as an eluate to obtain **11** as white crystals.

Yield 58.5%. mp 166–169 °C, lit [20], mp 166–168.5 °C. ^{1}H–NMR ($CDCl_3$): 4.28 (broad s, 4H, $N\underline{H}_2$), 5.01 (s, 2H, $OC\underline{H}_2$), 5.55 (s, 2H, aromatics), 7.38 (m, 5H, aromatics). MS: m/z 215. Found: 215.

6-Amino-2-(3-iodophenyl)-4-benzyloxy-3-(4-pyridyl)-*1H*-pyrrolo[2,3-b]pyridine (*m*-YTM) In DME (120 mL), **5a** (1.64 g) and **11** (0.77 g, 0.0036 mol) were dissolved, after which sulfuric acid (0.96 mL, 0.0181 mol) was added dropwise and refluxed for 6 h. After evaporating the solution under reduced pressure, an appropriate amount of methanol was added, and then the reaction was neutralized with sodium bicarbonate. After evaporating the product under reduced pressure, extracting with ethyl acetate, and washing with water, the organic layer was dried over sodium sulfate and then evaporated under reduced pressure. The residue was subjected to separation by silica gel column chromatography using chloroform, followed by chloroform/methanol (100/1, v/v) as eluates, and recrystallized with methanol to obtain *m*-YTM as yellow crystals.

Yield 44.1%. mp 296–298 °C. ^{1}H–NMR (DMSO): 5.02 (s, 2H, $OC\underline{H}_2$), 5.84 (s, 2H, $N\underline{H}_2$), 5.96 (s, 1H, $N\underline{H}$), 7.03 (t, J = 7.8 Hz, 1H, aromatics), 7.24 (d, J = 5.7 Hz, 2H, aromatics), 7.27 (m, 6H, aromatics), 7.54 (d, J = 7.8 Hz, 1H, aromatics), 7.62 (s, 1H, aromatics), 8.33 (d, J = 5.7 Hz, 2H, aromatics), 11.54 (s, 1H, aromatics). HRMS: m/z 518.0604. Found: 518.0602. Anal. calcd. for $C_{25}H_{19}IN_4O$: C, 57.93; H, 3.69; N, 10.81. Found: C, 57.23; H, 3.73; N, 10.53. IR(KBr): 3470, 3311, 1622, 1588, 1420, 1233 cm^{-1}.

6-Amino-2-(4-iodophenyl)-4-benzyloxy-3-(4-pyridyl)-*1H*-pyrrolo[2,3-b]pyridine (*p*-YTM) *p*-YTM was synthesized using **5b** by a method similar to that used for synthesizing *m*-YTM.

Yield 40.5%. mp 278–280 °C. ^{1}H–NMR (DMSO): 5.08 (s, 2H, $OC\underline{H}_2$), 5.87 (s, 2H, $N\underline{H}_2$), 6.02 (s, 1H, $N\underline{H}$), 7.09 (d, J = 8.4 Hz, 2H, aromatics), 7.19 (d, J = 3.3 Hz, 2H, aromatics), 7.29 (d, J = 5.7 Hz, 2H, aromatics), 7.35 (t, J = 3.3 Hz, 3H, aromatics), 7.67 (d, J = 8.4 Hz, 2H, aromatics), 8.36 (d, J = 5.7 Hz, 2H, aromatics), 11.58 (s, 1H, aromatics). HRMS: m/z 518.0604. Found: 518.0609. Anal. calcd. for $C_{25}H_{19}IN_4O$: C, 57.93; H, 3.69; N, 10.81. Found: C,57.14; H, 3.65; N, 10.35. IR(KBr): 3470, 3320, 1621, 1586, 1419, 1232 cm^{-1}.

6-Amino-2-(4-fluorophenyl)-4-benzyloxy-3-(4-pyridyl)-*1H*-pyrrolo[2,3-b]pyridine (RWJ-15) RWJ-15 was synthesized using **5c** by a method similar to that for synthesizing *m*-YTM.

Yield 42.3%. mp 275–276 °C, lit [21], mp 275–276 °C. HRMS: m/z 410.1543. Found: 410.1532.

Radiosynthesis (Scheme 4)

6-Amino-2-(3-tributylstanyl-phenyl)-4-benzyloxy-3-(4-pyridyl)-*1H*-pyrrolo[2,3-b]pyridine [12]

m-YTM (0.07 g, 0.14 mmol), bis(tributyltin) (0.21 mL, 0.42 mmol), and tetrakis (triphenylphosphine) palladium(0) (0.0085 g, 0.0074 mmol) were refluxed in anhydrous 1,4-dioxane (12 mL) overnight. After cooling, the reaction was filtered through Celite, and the filtrate was concentrated under reduced pressure. The residue was separated and purified by silica gel column chromatography using ethyl acetate/hexane (10/1, v/v) as an eluate to obtain **12** as yellow crystals.

Yield 31.4%. mp 160–165 °C. ^{1}H–NMR ($CDCl_3$): 0.86–1.47 (m, 27H, Bu_3), 4.01 (broad s, 2H, $N\underline{H}_2$), 5.05 (s, 2H, $OC\underline{H}_2$), 5.84 (s, 1H, $N\underline{H}$), 7.29 (m, 11H, aromatics), 8.32 (d, J = 6.0 Hz, 2H, aromatics), 10.61 (s, 1H, aromatics). MS: m/z 682. Found: 682.

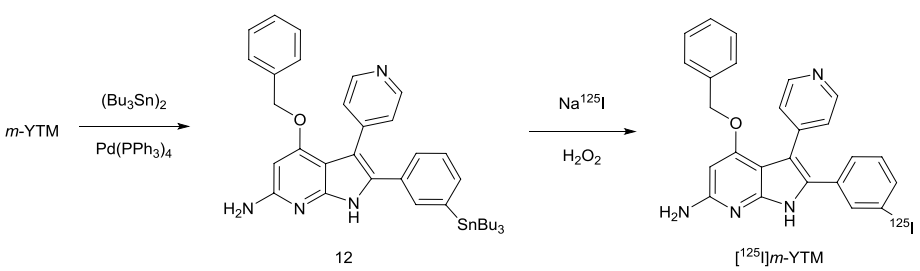

Scheme 4 Radiosynthesis of [^{125}I]*m*-YTM

6-Amino-2-(3-[^{125}I]iodophenyl)-4-benzyloxy-3-(4-pyridyl)-*1H*-pyrrolo[2,3-b]pyridine ([^{125}I]*m*-YTM) In a sealed vial, 99% ethanol (25 μL), 0.1 M HCl solution (25 μL), [^{125}I] sodium iodide (1 μL, 3.7 MBq), and 30% w/v hydrogen peroxide solution (10 μL), were sequentially added to precursor **12** (25 μL, 1 mg/ml methanol solution); the mixture was then allowed to react at room temperature for 10 min. A target compound was purified by HPLC using methanol/0.01 M phosphate buffer (80/20, v/v) as a mobile phase followed by radiochemical purity analysis.

Measurement of the inhibition of p38 phosphorylation by *m*, *p*-YTM

Assay dilution buffer (ADB: 20 mM MOPS-Na, 25 mM *β*-glycerol phosphate, 5 mM EGTA, 1 mM sodium orthovanadate, and 1 mM dithiothreitol; pH 7.2), Mg/ATP cocktail (500 μM cold ATP and 75 mM magnesium chloride in ADB), and [γ-^{32}P]ATP (0.2 μCi/μL in Mg/ATP cocktail) were prepared.

Myelin basic protein (20 μg) was suspended in the ADB (10 μL), and 10 μL of 5% DMSO 0.01 M HCl solution containing a test compound (*m*-YTM and RWJ-15: final concentration of 0.1 nM–1 μM; SB203580 and *p*-YTM: 1 nM–10 μM) was added. p38α (25 ng in 10 μL of ADB) and [γ-^{32}P]ATP (10 μL) were sequentially added and incubated at 30 °C for 30 min. After completion of the reaction, the reaction mixture was immediately spotted on P81 phosphocellulose paper. One minute later, the paper was washed three times with 0.75% phosphoric acid aqueous solution, once with acetone, and then dried well. Radioactivity was measured by a liquid scintillation counter after adding 10 mL of the Clear-sol I scintillator (Nacalai Tesque). Ten microliters of 5% DMSO 0.01 M HCl solution containing no sample was used as a control. The phosphorylation inhibition of each compound was expressed as a percentage relative to the control.

Binding of [^{125}I]*m*-YTM to the recombinant p38α

Sixty microliters of p38α (25 ng) suspension in ADB (pH 7.2) containing 0.1% Triton X-100 (Nacalai Tesque), 30 μL of 0.1% Triton X-100 1% DMSO solution, and 10 μL of [^{125}I]*m*-YTM in 0.1% Triton X-100 solution (1.67 kBq) were sequentially added to a total volume of 100 μL and incubated at 30 °C for 30 min. After the reaction, the solution was suction filtered using a glass filter and washed six times with 3 mL of ice-cold 0.2 mM phosphate buffer (pH 7.2). Subsequently, the radioactivity of the filter was measured by a gamma counter to measure the total amount of [^{125}I]*m*-YTM bound to p38. In a similar manner, the binding amounts with 30 μL of 0.1% Triton X-100 1% DMSO solution containing sample compounds (*m*-YTM, RWJ-15, SB203580, SB202190, SB202474, PD98059, U0126, SP600125, Go6985, and bisindolylmaleimide I at a final concentration of 1 μM) were measured and expressed as a percentage relative to the control.

Binding affinity of [^{125}I]*m*-YTM

To a 60-μL suspension of p38α (active or inactive form) (25 ng) in 0.1% Triton X-100 ADB (pH 7.2), 20 μL of 0.1% Triton X-100 and 1% DMSO solution with or without SB203580 (final concentration of 10 μM) was added. Further, a mixture containing 10 μL of *m*-YTM (final concentration of 1–100 nM) and 10 μL of 0.1% Triton X-100 containing [^{125}I]*m*-YTM (1.67 kBq) was added to make a total volume of 100 μL, and the resulting solution was incubated at 30 °C for 30 min. After the reaction, the solution was suction filtered using a glass filter and washed six times with 3 mL of ice-cold 0.2 mM phosphate buffer (pH 7.2). Subsequently, the radioactivity of the filter was measured by a gamma counter to determine the levels of total binding and nonspecific binding of [^{125}I]*m*-YTM to p38α (active or inactive form). The specific binding amount was determined by subtracting the nonspecific binding amount from the total binding amount at various concentrations. Kd and Bmax were calculated by Scatchard analysis on the basis of the obtained specific binding curves.

Cellular uptake study

Cancer cell lines were inoculated at 1.0×10^6 cells per 75 cm^2 dish and incubated in a CO_2 incubator (5% CO_2 at 37 °C, humidified), in accordance with a standard method. The media used were DMEM for A-375, B-16, C-6, and A-431; and RPMI 1640 for SLC, ME-180, and PC-3. A-431 was cultured with 5% FCS, and all others were cultured with medium containing 10% FCS supplemented with penicillin–streptomycin solution.

A-375 cells (1.0×10^6) were suspended in DMEM medium (5% FCS, 800 μL), and 100 μL of DMEM solution containing 5% DMSO with or without various sample compounds (*m*-YTM, RWJ-15, SB203580, SB202190, SB202474, PD98059, U0126, SP600125, Go6985, and bisindolylmaleimide I at a final concentration of 1 μM) was added to the suspension. To the mixed solution, 100 μL of 5% DMSO and 0.01 M HCl containing [^{125}I]*m*-YTM (1.08 kBq) was added to a total volume of 1 mL and incubated at 37 °C for 1 h. After the reaction, the solution was suction filtered using a glass filter and washed eight times with 3 mL ice-cold 0.2 mM phosphate buffer (pH 7.2). The amount of radioactivity accumulated in the cells over time was examined by measuring the radioactivity of the filter.

The accumulation of radioactivity was expressed as a percentage relative to the total binding amount of the control.

Various cancer cells (1.0×10^6) were suspended in medium (5% FCS, 800 µL), to which 100 µL of DMEM solution containing 5% DMSO with or without SB203580 (final concentration of 10 µM) was added. To this mixture, 100 µL of 5% DMSO and 0.01 M HCl containing [^{125}I]*m*-YTM (1.08 kBq) was added to make a total volume of 1 mL, which was then incubated at 37 °C for 1 h. After the reaction, the solution was suction filtered using a glass filter and washed eight times with 3 mL of ice-cold 0.2 mM phosphate buffer (pH 7.2). Subsequently, the amount of radioactivity accumulated in the cells was examined by measuring the radioactivity of the filter using a gamma counter.

In vivo biodistribution study

A suspension of B-16 cells (4×10^6 cells in 200 µL) was subcutaneously injected into the thigh of 4-week-old BALB/c-nu male nude mice (20–25 g) and raised for 2 weeks. [^{125}I]*m*-YTM (100 µL, 37 kBq in saline) was injected into the B-16 tumor-bearing mice via the tail vein. The mice were sacrificed over time and blood was collected; next, the tumor and each organ were excised to measure their weight and radioactivity. Radioactivity accumulation in each tissue was expressed as a percentage of the total dose per gram of tissue (% dose/g tissue).

Various tumor-bearing mice were generated to compare the accumulation dynamics of the compound in cancer tissues. Various cancer cell lines were suspended in a medium used for culture, and the numbers of cells per 200 µL of cell suspension were adjusted as follows: 5.0×10^6 for A-375, B-16, and SLC; and 1.0×10^7 for C-6, ME-180, A-431, and PC-3. A cell suspension of 200 µL was subcutaneously injected into the thigh of 4-week-old BALB/c-nu male nude mice (20–25 g) and raised for 2 weeks for the A-375, B-16, and SLC cell lines, 3 weeks for C-6 and A-431 cell lines, or 4 weeks for ME-180 and PC-3 cell lines, and mice with a tumor of approximately 1×1 cm were used for the experiment.

Statistical analysis

Data are presented as the mean ± standard deviation (S.D.). Statistical analysis was performed using the unpaired *t* test. A two-tailed value of $p < 0.05$ was considered statistically significant.

Results and discussion

Synthesis and radiosynthesis (Schemes 1, 2, 3, 4)

As shown in Fig. 1, in this study, we designed *m*-YTM and *p*-YTM based on a previous report of the structure–activity relationship which indicated possible introduction sites of a halogen atom in derivatives of RWJ-15 [19, 22]. Since the introduction of a large halogen atom on the *m* position reportedly contributed to high inhibitory potency toward p38α while RWJ-15 has a fluorine atom on the *p* position, we decided to test the possibilities of both *m*-YTM and *p*-YTM as a p38α imaging probe. In accordance with Schemes 1, 2, and 3 constructed following the previous report of RWJ-15 synthesis [19, 21, 23] with slight modifications, *m*-YTM, *p*-YTM, and RWJ-15 were successfully synthesized. On the other hand, *o*-YTM was not obtained in our preliminary synthetic trial probably due to a steric hindrance during a ring formation reaction shown in Scheme 3. Radioactive iodine labeling of *m*-YTM was performed by an organotin-radioactive iodine exchange reaction (Scheme 4). Based on the analytical HPLC following the labeling reaction, a single radioactive peak was observed at 19.1 min, consistent with the retention time of *m*-YTM; therefore, the peak was confirmed as [^{125}I]*m*-YTM. The radiochemical yield was 95.8%, the radiochemical purity was 99% or higher, and the molar activity was approximately 74.3 TBq/mmol.

Measurement of the inhibition of p38 phosphorylation by *m*, *p*-YTM

The calculated IC_{50} value was 4.8 nM for *m*-YTM, which corresponds to inhibitory activity comparable to that of the base compound RWJ-15 (2.6 nM). It was confirmed

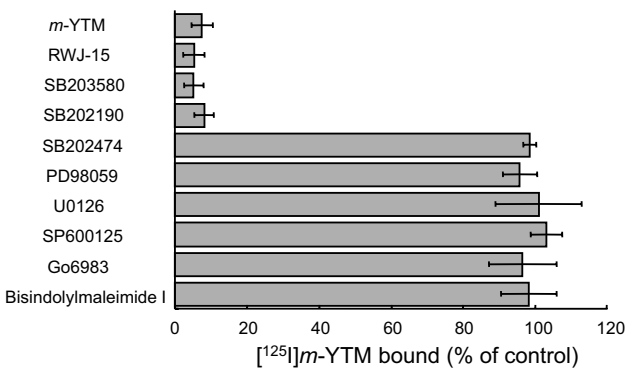

Fig. 2 Binding of [^{125}I]*m*-YTM to recombinant p38α with treatment of several inhibitors

that the inhibitory potency of *m*-YTM was about 13 times higher than a representative p38-selective inhibitor, SB203580 (63 nM). Meanwhile, the IC_{50} of *p*-YTM was 690 nM, which indicates lower potency than those of RWJ-15 and *m*-YTM; therefore, the results are consistent with that of a previous report [19, 22], which states that the inhibition of a derivative having a large halogen introduced at the *m* position is greater than that with a large halogen at the *p* position. Thus, it was proved that the method of drug design in this study was valid.

Binding of [^{125}I]*m*-YTM to the recombinant p38α (Fig. 2)

Because *m*-YTM exhibited excellent potential to inhibit p38 phosphorylation, the binding of the compound to p38α was examined. Human recombinant p38α was used as an enzyme sample. The amount of binding of [^{125}I]*m*-YTM upon pretreatment with various inhibitors [p38-selective inhibitors: RWJ-15, SB203580, and SB202190; p38 inactive analog: SB202474; MEK inhibitors: PD98059 and U0126; c-Jun N-terminal kinase (JNK) inhibitor: SP600125; Protein kinase C (PKC) inhibitors: Go6983 and bisindolylmaleimide I] was determined and expressed as a percentage relative to that of the control. The results indicated that the amount of [^{125}I]*m*-YTM binding to p38 was significantly lower than for the control upon pretreatment with p38-selective inhibitors such as RWJ-15, SB203580, and SB202190. Alternatively, no change was noted in the binding amount of [^{125}I]*m*-YTM when pretreated with a compound having no inhibitory activity toward p38, such as SB202474, PD98059, U0126, SP600125, Go6983, and bisindolylmaleimide I. Consequently, it was suggested that [^{125}I]*m*-YTM selectively binds to the recombinant p38α.

The binding affinity of [^{125}I]*m*-YTM (Fig. 3)

The cascade by which p38α transmits the signal from upstream into the nucleus comprises two stages, and p38α has two ATP binding pockets [24, 25]. Hence, two possibilities of p38α, activation site and autophosphorylation site, can be considered as candidates for the binding site of *m*-YTM that exhibits inhibitory activity toward p38α. We therefore performed a binding saturation assay using the active or inactive form of p38α to elucidate the binding site for *m*-YTM. The active form of p38α is a phosphorylated p38α which has the two active ATP binding pockets, activation site and autophosphorylation site, while the inactive form of p38α is a naïve p38α which has only one active ATP binding pocket, that is, activation site. The two forms of p38α protein could not be interconverted in the reaction solutions due to lack of a corresponding kinase. The specific binding amount of [^{125}I]*m*-YTM was calculated by using the

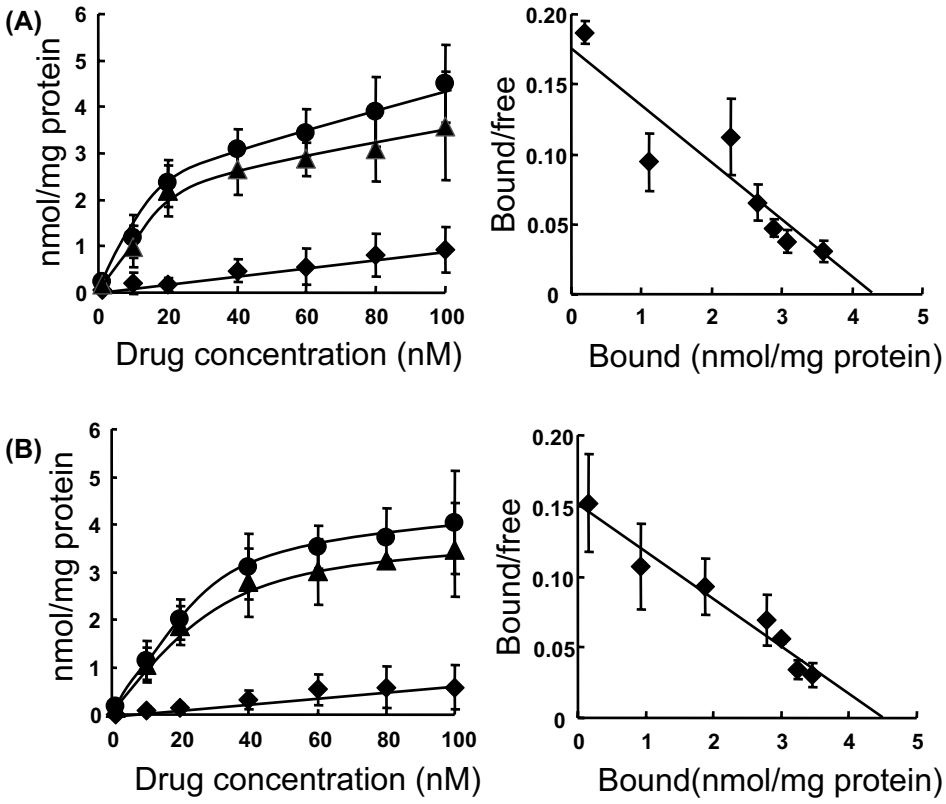

Fig. 3 Binding saturation assay of [^{125}I]*m*-YTM using active (A) and inactive (B) forms of p38α

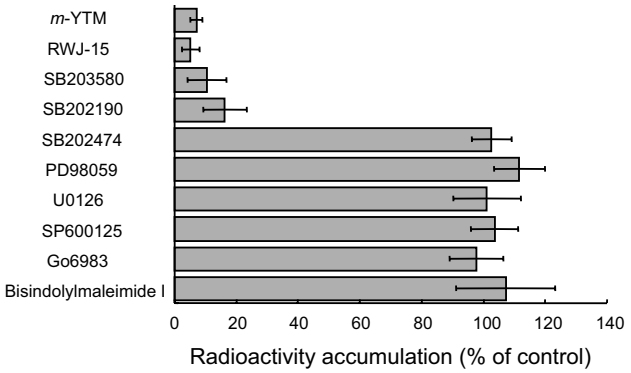

Fig. 4 Cellular uptake study of [^{125}I]*m*-YTM in A-375 cells with treatment of several inhibitors

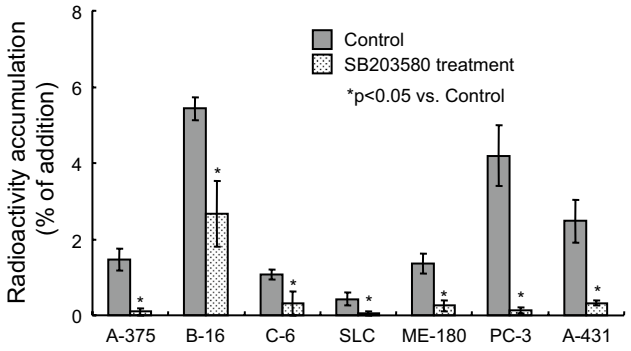

Fig. 5 Cellular uptake study of [^{125}I]*m*-YTM in several cancer cells with treatment of SB203580

active or inactive form of human recombinant p38α; next, the dissociation constant Kd and maximum binding number Bmax were calculated using the Scatchard analysis method.

The Kd value and the Bmax of *m*-YTM for activated p38α were 26.1 nM and 4.3 nmol/mg protein, respectively; those for inactivated p38α were 29.6 nM and 4.5 nmol/mg protein, respectively. *m*-YTM showed similar levels of binding affinities for active and inactive forms. Because the Hill coefficient was one for both, it was suggested that *m*-YTM has one binding site and there is no interaction with other binding sites. If *m*-YTM binds only to the active form, it would be considered to bind to an autophosphorylation site; if it binds to both active and inactive forms, it would be considered to bind to the p38α activation site. Therefore, it was suggested that the binding site of *m*-YTM is the p38α activation site, as in the case using the p38α-selective inhibitor SB203580 [26, 27]. Accordingly, the amount of *m*-YTM accumulated in cancer cells was considered to represent the amount of p38α present in the cells.

Table 1 Radioactivity biodistribution after intravenous administration of [^{125}I]*m*-YTM in B-16 cell-implanted model mice

	Time after administration (hours)			
	1	6	12	24
Blood	0.31 ± 0.07	0.06 ± 0.02	0.03 ± 0.01	0.02 ± 0.00
Pancreas	0.86 ± 0.13	0.07 ± 0.06	0.01 ± 0.01	0.00 ± 0.00
Spleen	1.24 ± 0.13	0.07 ± 0.07	0.03 ± 0.02	0.08 ± 0.08
Stomach	2.82 ± 1.57	0.32 ± 0.14	0.12 ± 0.14	0.07 ± 0.06
Liver	2.95 ± 0.36	0.98 ± 0.33	0.30 ± 0.07	0.32 ± 0.08
Kidney	3.42 ± 0.43	0.21 ± 0.11	0.10 ± 0.02	0.13 ± 0.02
Heart	0.43 ± 0.06	0.02 ± 0.02	0.00 ± 0.00	0.01 ± 0.01
Lung	0.84 ± 0.10	0.16 ± 0.04	0.07 ± 0.03	0.10 ± 0.04
Brain	0.05 ± 0.00	0.00 ± 0.00	0.00 ± 0.00	0.00 ± 0.00
Muscle	0.59 ± 0.21	0.02 ± 0.01	0.01 ± 0.02	0.01 ± 0.01
Tumor	1.79 ± 0.20	1.04 ± 0.15	0.98 ± 0.15	1.00 ± 0.08

Data are presented as % injected dose per gram. Each value represents the mean ± S.D. for four animals at each interval

Table 2 Tumor/blood and tumor/muscle ratios obtained from biodistribution studies of [^{125}I]*m*-YTM in a variety of tumor-implanted model mice

	Time after administration (hours)			
	Tumor/muscle ratio		Tumor/blood ratio	
	1	24	1	24
A-375	1.52 ± 0.25	1.47 ± 0.38	3.49 ± 0.41	0.91 ± 0.38
B-16	3.03 ± 0.28	47.6 ± 7.29	6.56 ± 1.32	213 ± 27.6
C-6	1.42 ± 0.81	0.92 ± 0.06	3.54 ± 1.84	1.11 ± 0.27
SLC	1.22 ± 0.24	5.88 ± 0.83	3.15 ± 0.59	1.87 ± 0.43
ME-180	1.06 ± 0.24	1.66 ± 0.24	1.38 ± 0.47	1.40 ± 1.41
PC-3	1.17 ± 0.09	2.43 ± 1.28	1.98 ± 0.35	0.84 ± 0.79
A-431	1.04 ± 0.16	7.11 ± 1.12	2.53 ± 0.15	3.24 ± 0.85

Each value represents the mean ± S.D. for four animals at each interval

Cellular uptake study (Figs. 4–5)

The cellular uptake of [^{125}I]*m*-YTM was examined using A-375 cells. The effects of various inhibitors were investigated by pretreating the cells and measuring the uptake of [^{125}I]*m*-YTM, which was determined as a percentage relative to that of the control. It was shown that the uptake of [^{125}I]*m*-YTM in A-375 cells was significantly decreased only with the p38α-selective inhibitors relative to that of the control, whereas the pretreatment with other inhibitors had no effect on the uptake amount. Accordingly, it was suggested that [^{125}I]*m*-YTM incorporated in the cancer cells selectively binds to p38α and is retained in the cells.

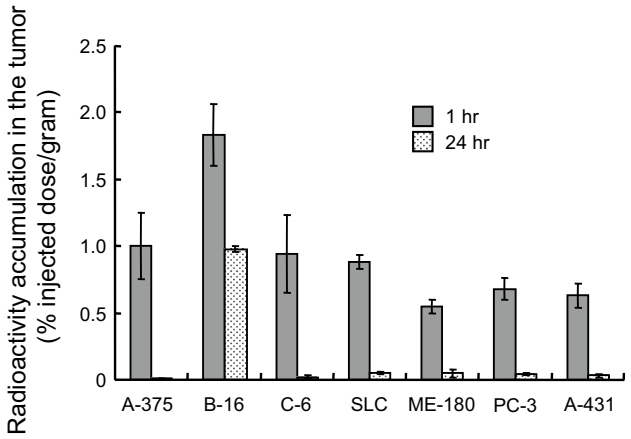

Fig. 6 Radioactivity accumulation in the tumor after intravenous administration of [^{125}I]*m*-YTM in a variety of tumor-implanted model mice

Then, the applicability of [^{125}I]*m*-YTM to various cancers was investigated. The cancer cell lines used were A-375 human malignant melanoma, B-16 mouse malignant melanoma, C6 rat brain tumor, SLC human lung tumor, ME-180 human cervical carcinoma, PC-3 human prostate cancer, and A-431 human squamous cell carcinoma. Using these cell lines, the uptake of [^{125}I]*m*-YTM was examined. The results revealed the uptake of [^{125}I]*m*-YTM in various cancer cells, which was significantly reduced by the p38α-selective inhibitor SB203580. Accordingly, it was suggested that [^{125}I]*m*-YTM is retained inside various cancer cells through the binding to p38α.

In vivo biodistribution study (Tables 1–2, Fig. 6)

In a study of pharmacokinetics of [^{125}I]*m*-YTM over time in B-16 tumor-bearing mice (Table 1), the radioactive accumulation in the tumor was 1.79% ID/g 1 h after administration, and was retained in the tumor for a long time; for example, even after 6, 12, and 24 h, it showed high accumulation of 1.04, 0.98, and 1.00% ID/g, respectively. Conversely, the liver and kidney showed high accumulation of 2.95 and 3.42% ID/g 1 h after the administration; however, the amount was decreased to lower than that in the tumor 6 h post-administration, and then continued to decrease over time. The accumulation in other organs was lower than that in the tumor starting from 1 h post-administration and it continued to decrease further thereafter. In particular, the accumulation was decreased to the background level 12 h post-administration and later, which confirms that [^{125}I]*m*-YTM has excellent excretion. In addition, it was suggested that [^{125}I]*m*-YTM is stably present in the body because low radioactivity accumulation in the stomach was observed, which is an index of deiodination.

The tumor to muscle ratio of radioactivity accumulation was 3.1 at 1 h post-administration, then increased over time, and reached a high value of more than 100 at 12 h post-administration. Similarly, the tumor to blood ratio was 5.8 at 1 h post-administration, and then increased further, reaching 50 at 24 h post-administration. The tumor to liver and tumor to kidney ratios were 3.2 and 9.5 at 12 h post-administration, respectively. The tumor to lung ratio was 14.2 at 12 h post-administration, and the tumor to stomach ratio was as high as 15.1 at 24 h post-administration.

The accumulation of [^{125}I]*m*-YTM in the tumor was examined using various tumor-bearing mice (Table 2, Fig. 6). At 1 h post-administration, the accumulation ranged from 0.55 to 1.84% ID/g. In B-16-bearing mice, the accumulation was 1.00% ID/g at 24 h post-administration; however, it was 0.01%–0.05% ID/g in other cancer tissues. The reason for the difference in the radioactivity accumulations between B-16 and other tumors remained unsolved, but somehow might be attributed to binding with an indeterminate factor different from those evaluated in Fig. 4, and not to non-specific retention. This is because the contribution of p38α specific accumulation on B-16 radioactivity was estimated approximately a half from the cellular uptake study in Fig. 5. Therefore, the elucidation of this issue and further quantitative assessment of the radioactivity accumulation profile corresponding to the expression and activity levels of p38α would be demanded in future. Nevertheless, the ratios of accumulation in the tumor to that in blood and in tumor to that in muscle were ≥ 1 at 1 h post-administration in all tumors tested; therefore, [^{125}I]*m*-YTM seems to be applicable to various types of cancer. Cumulatively, these findings suggest that [^{125}I]*m*-YTM is an effective p38α imaging probe that can be employed for different types of tumor.

p38α is a ubiquitous protein kinase activated in response to external stimuli and is closely implicated in the modulation of multiple cellular processes such as apoptosis [5, 6]. Also, p38α is recognized as a potential therapeutic target because of contribution on the progression of tumors [17, 18]. Therefore, [^{123}I]*m*-YTM can be an effective imaging probe for usefulness evaluation of such p38α specific targeting agents as well as therapeutic agents targeting other kinases or receptors locating in the upstream of the p38α pathway in view of the final therapeutic effects. In addition, [^{123}I]*m*-YTM would have a great potential for the diagnosis of a broad range of diseases such as cancers and ischemic diseases that activate the p38α pathway.

Funding This work was partly supported by a Grant-in-Aid for Scientific Research from the Japan Society for the Promotion of Science (No. 12770512). There are no conflicts of interest.

References

1. Marshall CJ. MAP kinase kinase kinase, MAP kinase kinase and MAP kinase. Curr Opin Genet Dev. 1994;4(1):82–9.
2. Nishida E, Gotoh Y. The MAP kinase cascade is essential for diverse signal transduction pathways. Trends Biochem Sci. 1993;18(4):128–31.
3. Kyriakis JM, Avruch J. Protein kinase cascades activated by stress and inflammatory cytokines. BioEssays. 1996;18(7):567–77.
4. New L, Han J. The p38 MAP kinase pathway and its biological function. Trends Cardiovasc Med. 1998;8(5):220–8.
5. Lo U, Selvaraj V, Plane JM, Chechneva OV, Otsu K, Deng W. p38alpha (MAPK14) critically regulates the immunological response and the production of specific cytokines and chemokines in astrocytes. Sci Rep. 2014;4:7405.
6. Sui X, Kong N, Ye L, Han W, Zhou J, Zhang Q, et al. p38 and JNK MAPK pathways control the balance of apoptosis and autophagy in response to chemotherapeutic agents. Cancer Lett. 2014;344(2):174–9.
7. Bogoyevitch MA, Gillespie-Brown J, Ketterman AJ, Fuller SJ, Ben-Levy R, Ashworth A, et al. Stimulation of the stress-activated mitogen-activated protein kinase subfamilies in perfused heart. p38/RK mitogen-activated protein kinases and c-Jun N-terminal kinases are activated by ischemia/reperfusion. Circ Res. 1996;79(2):162–73.
8. Ma XL, Kumar S, Gao F, Louden CS, Lopez BL, Christopher TA, et al. Inhibition of p38 mitogen-activated protein kinase decreases cardiomyocyte apoptosis and improves cardiac function after myocardial ischemia and reperfusion. Circulation. 1999;99(13):1685–91.
9. Yue TL, Wang C, Gu JL, Ma XL, Kumar S, Lee JC, et al. Inhibition of extracellular signal-regulated kinase enhances Ischemia/Reoxygenation-induced apoptosis in cultured cardiac myocytes and exaggerates reperfusion injury in isolated perfused heart. Circ Res. 2000;86(6):692–9.
10. Sugino T, Nozaki K, Takagi Y, Hattori I, Hashimoto N, Moriguchi T, et al. Activation of mitogen-activated protein kinases after transient forebrain ischemia in gerbil hippocampus. J Neurosci. 2000;20(12):4506–14.
11. Walton KM, DiRocco R, Bartlett BA, Koury E, Marcy VR, Jarvis B, et al. Activation of p38MAPK in microglia after ischemia. J Neurochem. 1998;70(4):1764–7.
12. Barancik M, Htun P, Strohm C, Kilian S, Schaper W. Inhibition of the cardiac p38-MAPK pathway by SB203580 delays ischemic cell death. J Cardiovasc Pharmacol. 2000;35(3):474–83.
13. Mackay K, Mochly-Rosen D. An inhibitor of p38 mitogen-activated protein kinase protects neonatal cardiac myocytes from ischemia. J Biol Chem. 1999;274(10):6272–9.
14. Symes K, Mercola M. Embryonic mesoderm cells spread in response to platelet-derived growth factor and signaling by phosphatidylinositol 3-kinase. Proc Natl Acad Sci USA. 1996;93(18):9641–4.
15. Han Q, Leng J, Bian D, Mahanivong C, Carpenter KA, Pan ZK, et al. Rac1-MKK3-p38-MAPKAPK2 pathway promotes urokinase plasminogen activator mRNA stability in invasive breast cancer cells. J Biol Chem. 2002;277(50):48379–85.
16. Huang S, New L, Pan Z, Han J, Nemerow GR. Urokinase plasminogen activator/urokinase-specific surface receptor expression and matrix invasion by breast cancer cells requires constitutive p38alpha mitogen-activated protein kinase activity. J Biol Chem. 2000;275(16):12266–72.
17. Igea A, Nebreda AR. The stress kinase p38alpha as a target for cancer therapy. Cancer Res. 2015;75(19):3997–4002.
18. Koul HK, Pal M, Koul S. Role of p38 MAP kinase signal transduction in solid tumors. Genes Cancer. 2013;4(9–10):342–59.
19. Henry JR, Rupert KC, Dodd JH, Turchi IJ, Wadsworth SA, Cavender DE, et al. Potent inhibitors of the MAP kinase p38. Bioorg Med Chem Lett. 1998;8(23):3335–40.
20. Markees DG, Dewey VC, Kidder GW. The synthesis and biological activity of substituted 2,6-diaminopyridines. J Med Chem. 1968;11(1):126–9.
21. Henry JR, Rupert KC, Dodd JH, Turchi IJ, Wadsworth SA, Cavender DE, et al. 6-Amino-2-(4-fluorophenyl)-4-methoxy-3-(4-pyridyl)-1H-pyrrolo[2, 3-b]pyridine (RWJ 68354): a potent and selective p38 kinase inhibitor. J Med Chem. 1998;41(22):4196–8.
22. Wilson KP, McCaffrey PG, Hsiao K, Pazhanisamy S, Galullo V, Bemis GW, et al. The structural basis for the specificity of pyridinylimidazole inhibitors of p38 MAP kinase. Chem Biol. 1997;4(6):423–31.
23. Henry JR, Dodd JH. Synthesis of RWJ 68354: a potent inhibitor of the MAP kinase p38. Tetrahedron Lett. 1998;39(48):8763–4.
24. Cohen P. The search for physiological substrates of MAP and SAP kinases in mammalian cells. Trends Cell Biol. 1997;7(9):353–61.
25. Moriguchi T, Gotoh Y, Nishida E. Roles of the MAP kinase cascade in vertebrates. Adv Pharmacol. 1996;36:121–37.
26. Han H, Wang H, Long H, Nattel S, Wang Z. Oxidative preconditioning and apoptosis in L-cells. Roles of protein kinase B and mitogen-activated protein kinases. J Biol Chem. 2001;276(28):26357–64.
27. Xia Z, Dickens M, Raingeaud J, Davis RJ, Greenberg ME. Opposing effects of ERK and JNK-p38 MAP kinases on apoptosis. Science. 1995;270(5240):1326–31.